Reduced Myogenic and Increased Adipogenic Differentiation Capacity of Rotator Cuff Muscle Stem Cells

Manuel F. Schubert, MD, MS, Andrew C. Noah, MS, Asheesh Bedi, MD, Jonathan P. Gumucio, PhD, and Christopher L. Mendias, PhD, ATC

Investigation performed at the University of Michigan Medical School, Ann Arbor, Michigan

Background: Fat accumulation commonly occurs in chronically torn rotator cuff muscles, and increased fat within the rotator cuff is correlated with poor clinical outcomes. The extent of lipid deposition is particularly pronounced in injured rotator cuff muscles compared with other commonly injured muscles such as the gastrocnemius. Satellite cells, which are a tissue-resident muscle stem-cell population, can differentiate into fat cells. We hypothesized that satellite cells from the rotator cuff have greater intrinsic adipogenic differentiation potential than do gastrocnemius satellite cells, and this difference is due to variations in epigenetic imprinting between the cells.

Methods: Satellite cells from gastrocnemius and rotator cuff muscles of mice were cultured in adipogenic media, and the capacity to differentiate into mature muscle cells and adipogenic cells was assessed ($n \geq 9$ plates per muscle group). We also performed DNA methylation analysis of gastrocnemius and rotator cuff satellite cells to determine whether epigenetic differences were present between the 2 groups ($n = 5$ mice per group).

Results: Compared with the gastrocnemius, satellite cells from the rotator cuff had a 23% reduction in myogenic differentiation and an 87% decrease in the expression of the differentiated muscle cell marker MRF4 (myogenic regulatory factor 4). With respect to adipogenesis, rotator cuff satellite cells had a 4.3-fold increase in adipogenesis, a 12-fold increase in the adipogenic transcription factor PPARγ (peroxisome proliferator-activated receptor gamma), and a 65-fold increase in the adipogenic marker FABP4 (fatty-acid binding protein 4). Epigenetic analysis identified 355 differentially methylated regions of DNA between rotator cuff and gastrocnemius satellite cells, and pathway enrichment analysis suggested that these regions were involved with lipid metabolism and adipogenesis.

Conclusions: Satellite cells from rotator cuff muscles have reduced myogenic and increased adipogenic differentiation potential compared with gastrocnemius muscles. There appears to be a cellular and genetic basis behind the generally poor rates of rotator cuff muscle healing.

Clinical Relevance: The reduced myogenic and increased adipogenic capacity of rotator cuff satellite cells is consistent with the increased fat content and poor muscle healing rates often observed for chronically torn rotator cuff muscles. For patients undergoing rotator cuff repair, transplantation of autologous satellite cells from other muscles less prone to fatty infiltration may improve clinical outcomes.

Rotator cuff tears are a common upper-extremity disorder, with >250,000 surgical repairs performed annually in the U.S.[1]. Achieving positive clinical outcomes following repair can be limited by fatty infiltration or myosteatosis, which is the combined atrophy, fibrosis, and fat accumulation within and around myofibers[2-4]. The relative amount of fat in torn rotator cuff muscles is often greater than in other injured muscle groups[5-7], and many patients develop further myosteatosis even after undergoing a successful rotator cuff repair[2]. Fat accumulation is also correlated with negative clinical

Disclosure: Funding support for this study was provided by the Orthopaedic Research and Education Foundation and NIH grant F31-AR065931. On the **Disclosure of Potential Conflicts of Interest** forms, *which are provided with the online version of the article,* one or more of the authors checked "yes" to indicate that the author had a relevant financial relationship in the biomedical arena outside the submitted work and "yes" to indicate that the author had other relationships or activities that could be perceived to influence, or have the potential to influence, what was written in this work (http://links.lww.com/JBJS/F34).

outcomes[2,8], and identifying the cellular and molecular mechanisms that induce adipogenesis in the rotator cuff could provide new opportunities for improving muscle healing and recovery.

Satellite cells are a heterogenous stem-cell population largely responsible for postnatal skeletal muscle growth, regeneration, and repair, and they are stimulated by trauma to proliferate, differentiate, and fuse into damaged myofibers[9,10]. Quiescent satellite cells are found between the muscle fibers and basal lamina and express the transcription factor Pax7 (paired box 7)[10,11]. In addition to myofibers, satellite cells can also differentiate into adipocytes[12-14], and in a tenotomy and denervation muscle-injury model, greater fat accumulation and reduced healing were present in rotator cuff muscles compared with gastrocnemius muscles[7]. Because satellite cells are important in muscle regeneration and can enter the adipogenic lineage, we sought to determine differences in the myogenic and adipogenic differentiation capacity of satellite cells from gastrocnemius and rotator cuff muscles. We tested the hypothesis that, compared with gastrocnemius satellite cells, rotator cuff satellite cells have decreased myogenic and increased adipogenic differentiation capacity. To further explore mechanistic differences, as satellite cell activity can be regulated by epigenetic factors[11], we analyzed differential DNA methylation between gastrocnemius and rotator cuff satellite cells.

Materials and Methods

Animals

This study was approved by the University of Michigan Institutional Animal Care and Use Committee. We crossed 2 lines of genetically modified mice, obtained from The Jackson Laboratory, to generate experimental animals. First, we obtained $Pax7^{CreERT2}$ mice, which contain an IRES (internal ribosome entry site)-CreERT2 cassette between the stop codon and 3′ untranslated region of Pax7, resulting in the expression of a tamoxifen-responsive CreERT2 recombinase enzyme when Pax7 is also expressed (strain

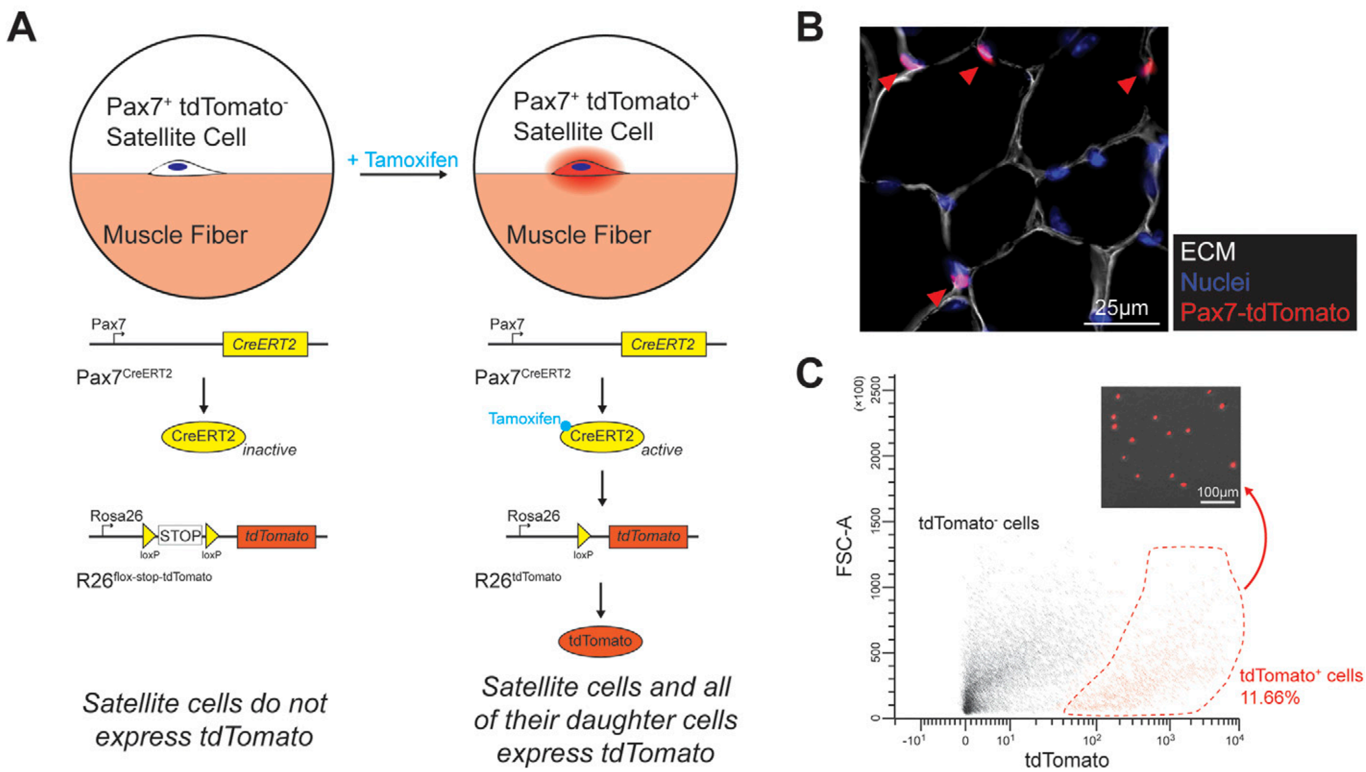

Fig. 1
Overview of genetically modified mice, satellite cell labeling, and sorting. **Fig. 1-A** $Pax7^{CreERT2}$:$R26^{flox\text{-}stop\text{-}tdTomato}$ mice do not normally express the red fluorescent protein tdTomato. When CreERT2 in Pax7^{+} satellite cells is activated in response to tamoxifen treatment, the stop codon cassette flanked by loxP sites is excised from the constitutively active Rosa26 (R26R) locus, causing tdTomato to be expressed in satellite cells, as well as in all subsequent daughter cells ($Pax7^{CreERT2}$:$R26^{tdTomato}$ mice). **Fig. 1-B** Representative histology of muscles from tamoxifen-treated $Pax7^{CreERT2}$:$R26^{tdTomato}$ mice, demonstrating the presence of tdTomato in satellite cells (red arrowheads). White = extracellular matrix (ECM) as marked by WGA-lectin, blue = nuclei, and red = Pax7-tdTomato. **Fig. 1-C** Representative flow sorting of tdTomato^{+} cells, plotted as forward scatter area (FSC-A) versus tdTomato fluorescent intensity, with the dashed area indicating the cells used for in vitro cell culture and DNA methylation sequencing studies. The inset is of an aliquot of the sorted cells demonstrating the visualization of viable tdTomato^{+} cells, visualized by overlaying the red fluorescent image onto the phase contrast image.

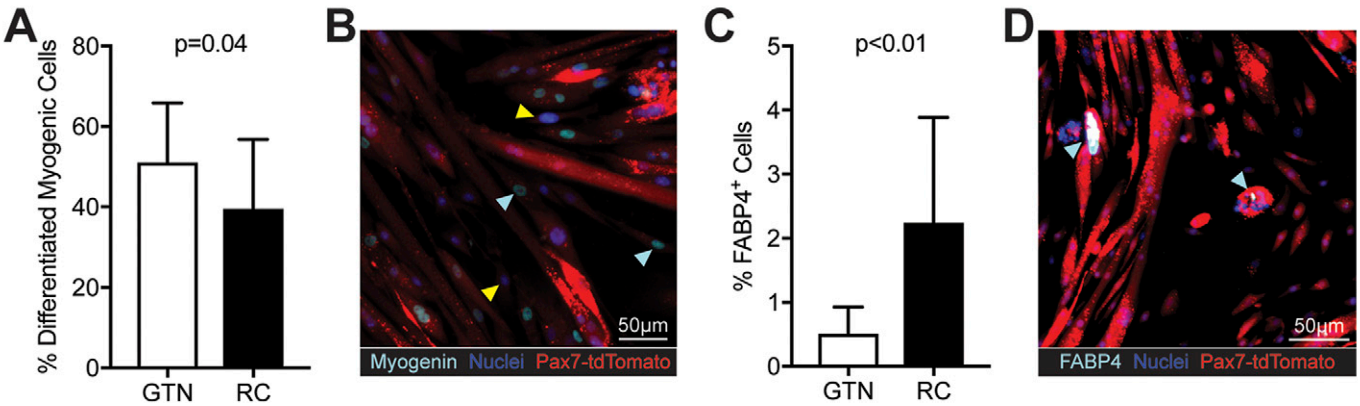

Fig. 2

Immunocytochemistry results. **Fig. 2-A** The percentage of differentiated muscle cells as a fraction of total cells per field for gastrocnemius (GTN) and rotator cuff (RC) groups. **Fig. 2-B** Representative image of myogenin-expressing cells. Teal = myogenin, blue = nuclei, and red = Pax7-tdTomato. The teal arrowheads illustrate myogenin$^+$ nuclei, and the yellow arrowheads are examples of myogenin$^-$ nuclei in mononuclear cells. **Fig. 2-C** The percentage of adipogenic FABP4$^+$ cells as a fraction of total cells per field for gastrocnemius (GTN) and rotator cuff (RC) groups. **Fig. 2-D** Representative image of FABP4-expressing cells. Teal = FABP4, blue = nuclei, and red = Pax7-tdTomato. Teal arrowheads are examples of FABP4$^+$ cells. N ≥ 9 plates analyzed per group. Values are mean and standard deviation.

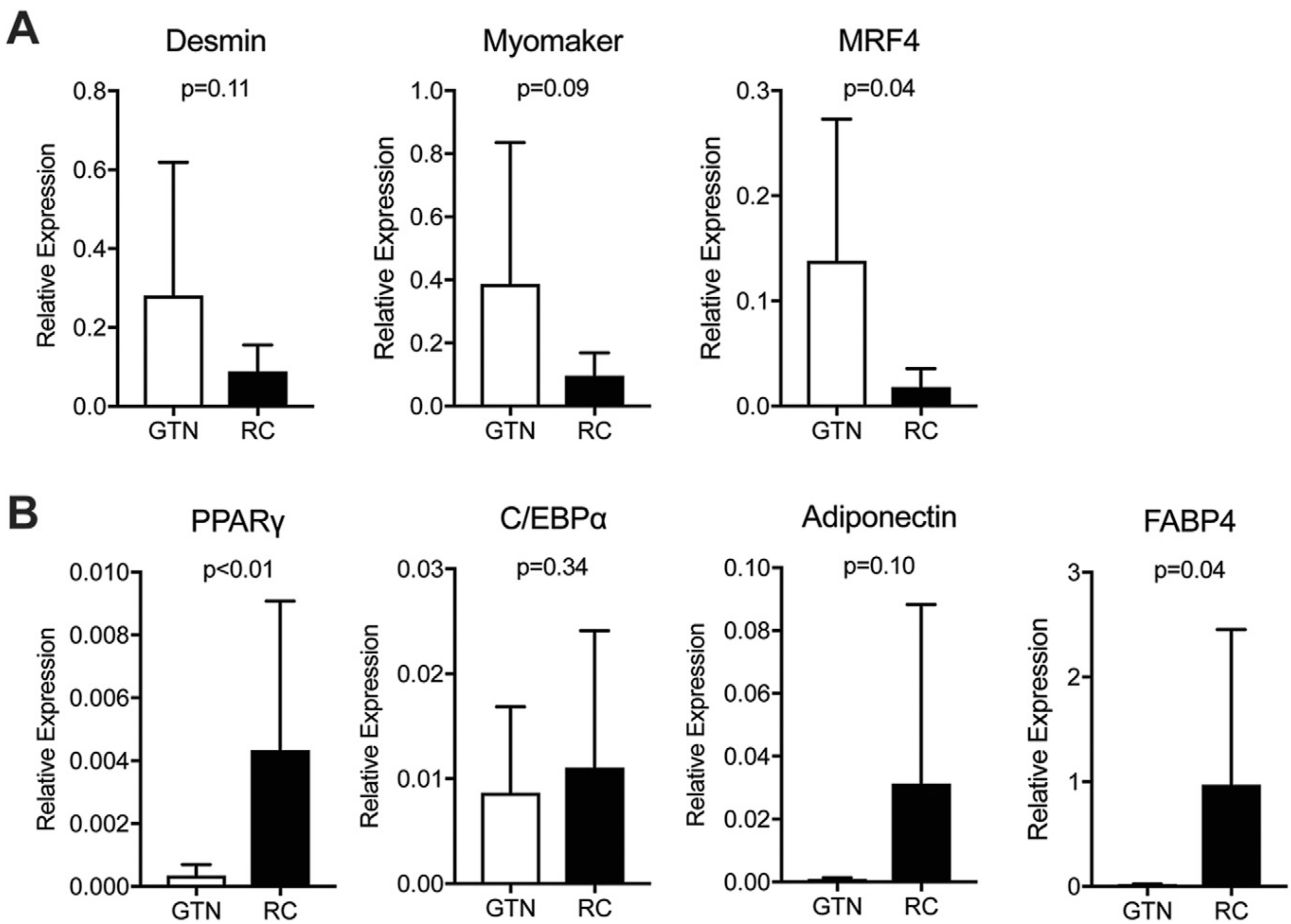

Fig. 3

Gene expression. Quantification of the expression of myogenic genes (**Fig. 3-A**) and adipogenic genes (**Fig. 3-B**). Each target gene normalized to the stable housekeeping gene β2-microglobulin. Values are presented as the mean and standard deviation; n ≥ 6 plates analyzed per group. MRF4 = myogenic regulatory factor 4, PPARγ = peroxisome proliferator-activated receptor gamma, C/EBPα = CCAAT-enhancer-binding protein-alpha, and FABP4 = fatty-acid binding protein 4.

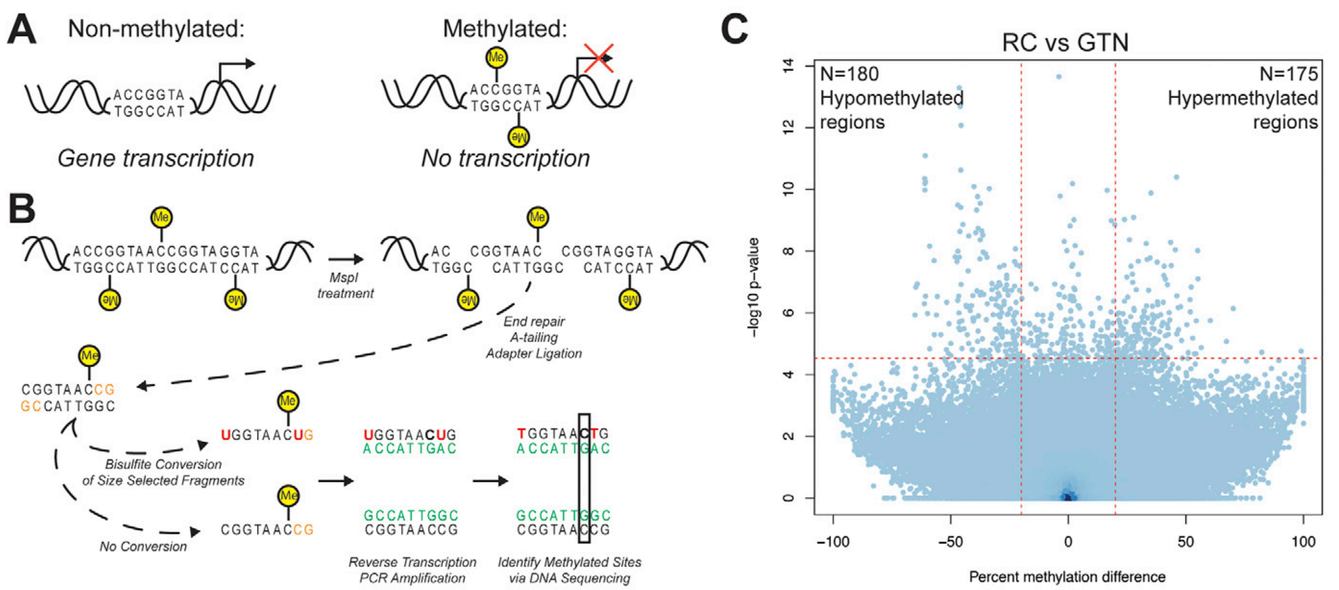

D

Biological Process	p-value
Appendage morphogenesis	0.0002
Limb morphogenesis	0.0002
Appendage development	0.00039
Limb development	0.00039
Anterior/posterior pattern specification	0.00058
Embryonic skeletal system development	0.00063
Embryonic morphogenesis	0.00073
Regionalization	0.00168
Pattern specification process	0.0017
Embryonic organ morphogenesis	0.00172
Mechanoreceptor differentiation	0.00282
Skeletal system development	0.00304
Embryonic limb morphogenesis	0.00473
Embryonic appendage morphogenesis	0.00473
Positive regulation of transcription from RNA polymerase II promoter	0.00485

E

Molecular Function	p-value
Sequence-specific DNA binding	0.00003
DNA binding	0.00098
Sequence-specific double-stranded DNA binding	0.00325
O-acyltransferase activity	0.0041
Glycerol-3-phosphate O-acyltransferase activity	0.00601
1-phosphatidylinositol binding	0.00601
Nucleosome binding	0.00601
Double-stranded DNA binding	0.00765
Nucleic acid binding	0.00766
RNA polymerase II regulatory region DNA binding	0.00829
Transcription regulatory region sequence-specific DNA binding	0.01017
Acylglycerol O-acyltransferase activity	0.01711
HMG box domain binding	0.01711
Heterocyclic compound binding	0.01791
DNA binding transcription factor activity	0.01822

Fig. 4

DNA methylation analysis. **Figs. 4-A and 4-B** Overview of DNA methylation (Me) and the enhanced reduced representation bisulfite sequencing process. **Fig. 4-A** When cytosine is methylated in regulatory regions, gene transcription is blocked. **Fig. 4-B** Overview of DNA digestion, bisulfite conversion, polymerase chain reaction (PCR) amplification, and sequencing to determine methylated cytosine residues. **Fig. 4-C** Volcano plot demonstrating differences between the gastrocnemius (GTN) and rotator cuff (RC) groups in differentially methylated regions (DMRs). **Figs. 4-D and 4-E** Gene ontology analysis of relevant biological processes and molecular function predictions of DMR data. N = 5 mice per group. HMG = high mobility group.

017763)[15]. In the second line of mice, *R26R^flox-stop-tdTomato^*, the constitutively expressed Rosa26 (R26R) locus was modified to contain a stop codon cassette flanked by loxP sites upstream of the red fluorescent tdTomato gene (strain 007909)[16]. In the absence of active Cre recombinase, *R26R^flox-stop-tdTomato^* mice do not express tdTomato. However, upon treatment with tamoxifen, which activates the Cre enzyme, a recombination event occurs between loxP sites to remove the stop codons, resulting in the permanent expression of tdTomato, *R26R^tdTomato^*. We crossed *Pax7^CreERT2^* and *R26R^flox-stop-tdTomato^* mice to generate *Pax7^CreERT2^:R26R^flox-stop-tdTomato^* mice, which were backcrossed for several generations and maintained in the homozygous state. Quiescent satellite cells express Pax7[15], and upon treatment with tamoxifen, the CreERT2 enzyme complex is activated, causing a recombination event at the R26R locus, resulting in the persistent expression of tdTomato in all cells expressing Pax7, as well as their daughter cells[17], which are referred to as *Pax7^CreERT2^:R26R^tdTomato^* mice. An overview is presented in Figure 1-A. With the exception of wild-type C57Bl/6 mice that were used to determine baseline flow cytometry fluorescence, all experiments utilized 4-month-old male *Pax7^CreERT2^:R26R^tdTomato^* mice.

The labeling of satellite cells with tdTomato occurred by treating mice with an intraperitoneal injection of tamoxifen (2 mg) dissolved in corn oil (Sigma) daily for 5 days prior to muscle harvest. On the sixth day, mice were anesthetized with ketamine and xylazine. The supraspinatus and infraspinatus muscles of the rotator cuff and the gastrocnemius muscles were removed and processed for flow cytometry. The plantaris muscle was also removed as a sentinel to verify recombination and labeling of satellite cells. Following muscle removal, mice were killed by cervical dislocation and pneumothorax.

Muscle Histology

Plantaris muscles were frozen in Tissue-Tek (Sakura) with cold isopentane, and 10-μm sections were incubated with

TABLE I Top 50 Differentially Hypermethylated Regions of DNA in Satellite Cells from the Rotator Cuff Compared with the Gastrocnemius

ID	Symbol	Gene Name	Methylation Difference *(%)*	Distance *(bp)*	P Value
NM_001113412	Fggy	FGGY carbohydrate kinase domain containing	99.03	177,851	0.035
NR_046076	Gm4251	Predicted gene 4251	82.28	33,232	0.038
NM_025642	Mis18a	MIS18 kinetochore protein A	70.18	45,772	0.004
NM_025642	Mis18a	MIS18 kinetochore protein A	67.24	45,822	0.021
NM_029441	Cdyl2	Chromodomain protein, Y chromosome-like 2	60.33	183,549	0.007
NM_013813	Epb41l3	Erythrocyte membrane protein band 4.1 like 3	56.46	196,484	0.029
NM_198610	Igsf21	Immunoglobulin superfamily, member 21	55.18	0	0.001
NM_001286033	Stx2	Syntaxin 2	55.06	280,368	<0.001
NM_001286033	Stx2	Syntaxin 2	54.42	280,443	0.008
NM_015803	Atp8a2	ATPase, aminophospholipid transporter-like, class I, type 8A, member 2	54.25	48,132	0.040
NM_001033228	Itga1	Integrin alpha 1	53.62	245,091	0.040
NM_015803	Atp8a2	ATPase, aminophospholipid transporter-like, class I, type 8A, member 2	52.84	48,082	0.018
NM_001033228	Itga1	Integrin alpha 1	52.23	245,041	0.001
NM_029441	Cdyl2	Chromodomain protein, Y chromosome-like 2	51.93	183,449	0.005
NR_024085	BC006965	cDNA sequence BC006965	51.80	1,001,517	0.003
NM_029441	Cdyl2	Chromodomain protein, Y chromosome-like 2	50.96	183,424	0.038
NR_030709	Gm16386	Predicted gene 16386	50.32	41,229	0.009
NR_015496	1700031M16Rik	RIKEN cDNA 1700031M16 gene	48.16	9,442	0.021
NM_152895	Kdm5b	Lysine (K)-specific demethylase 5B	47.71	0	0.004
NM_152895	Kdm5b	Lysine (K)-specific demethylase 5B	46.90	0	0.012
NM_198610	Igsf21	Immunoglobulin superfamily, member 21	46.79	0	0.004
NM_009723	Atp2b2	ATPase, Ca++ transporting, plasma membrane 2	46.16	0	0.015
NR_015496	1700031M16Rik	RIKEN cDNA 1700031M16 gene	46.08	9,267	0.002
NR_015496	1700031M16Rik	RIKEN cDNA 1700031M16 gene	46.07	9,292	0.015
NM_010462	Hoxc10	Homeobox C10	45.99	717	<0.001
NM_010462	Hoxc10	Homeobox C10	45.53	692	<0.001
NR_131145	Gm29683	Predicted gene 29683	43.80	351,254	<0.001
NM_177544	Ang4	Angiogenin, ribonuclease A family, member 4	43.46	20,976	<0.001
NM_180662	Trappc9	Trafficking protein particle complex 9	43.22	0	0.029
NR_102286	4933432K03Rik	RIKEN cDNA 4933432K03 gene	43.10	37,697	0.007
NM_009834	Noct	Nocturnin	42.86	19,402	0.005
NM_172462	Zfp11	Zinc finger protein 11	42.51	187,078	0.015
NR_131145	Gm29683	Predicted gene 29683	42.34	351,279	0.011
NR_102286	4933432K03Rik	RIKEN cDNA 4933432K03 gene	42.18	37,647	0.009
NM_177544	Ang4	Angiogenin, ribonuclease A family, member 4	42.14	20,901	0.001
NR_045702	AW549542	Expressed sequence AW549542	42.10	21,482	0.049
NM_009834	Noct	Nocturnin	42.05	19,377	0.026
NM_001310738	Siglech	Sialic acid binding Ig-like lectin H	41.27	26,345	0.001
NR_035497	Mir1970	MicroRNA 1970	41.20	0	0.016
NM_180662	Trappc9	Trafficking protein particle complex 9	40.80	0	<0.001
NM_001029872	Itgad	Integrin, alpha D	40.64	22,757	0.001
NM_009834	Noct	Nocturnin	40.48	19,327	0.042

continued

TABLE I (*continued*)

ID	Symbol	Gene Name	Methylation Difference *(%)*	Distance *(bp)*	P Value
NM_001042617	Cadps	Ca2+-dependent secretion activator	40.33	0	0.003
NM_009309	T	Brachyury, T-box transcription factor T	40.30	0	0.008
NM_027188	Smyd3	SET and MYND domain containing 3	39.79	0	0.010
NM_009309	T	Brachyury, T-box transcription factor T	39.59	0	0.033
NM_015764	Greb1	Gene regulated by estrogen in breast cancer protein	39.20	0	0.005
NR_038085	Six3os1	SIX homeobox 3, opposite strand 1	38.87	66,806	0.013
NR_045342	4933411E08Rik	RIKEN cDNA 4933411E08 gene	38.21	0	0.020
NM_013723	Podxl	Podocalyxin-like	38.01	246,814	0.003

wheat germ agglutinin (WGA) lectin conjugated to Alexa Fluor 488 dye (ThermoFisher Scientific) to identify extracellular matrix. DAPI (4′,6-diamidino-2-phenylindole; Sigma)-labeled nuclei and tdTomato-identified satellite cells. Sections were visualized with a BX51 microscope (Olympus).

Satellite Cell Isolation and Flow Cytometry

Satellite cells were isolated from gastrocnemius and rotator cuff muscles, using a method modified from a previous report[18]. A detailed description is provided in the Appendix. Briefly, muscles were minced and digested to generate a suspension of cells enriched with satellite cells. Cells were then sorted via flow cytometry on the basis of forward scatter area (FSC-A) as a means to measure the cell size and tdTomato fluorescence. TdTomato$^+$ cells were collected and used for in vitro differentiation experiments or DNA sequencing.

Cell Culture

A detailed description of cell culture is provided in the Appendix. Sorted cells were plated on culture dishes coated with growth factor-reduced Matrigel (Corning). Cells were expanded in growth media containing Dulbecco modified Eagle medium (DMEM) with 10% fetal bovine serum (FBS) and 1% antibiotic-antimycotic (AbAm) (ThermoFisher Scientific) for 2 passages, and on reaching 70% confluence, were switched to adipogenic induction media for a period of 7 days prior to immunocytochemistry and gene-expression analysis[14,19].

Immunocytochemistry

Cells were fixed with 4% paraformaldehyde, permeabilized in 0.5% Triton X-100, and blocked in 5% goat serum. Cells were labeled with antibodies against myogenin (F5D, 1:100; Developmental Studies Hybridoma Bank), which is a transcription factor that identifies differentiated muscle cells[20,21], or with antibodies against fatty-acid binding protein 4 (FABP4, 1:500; AbCam), which is specifically expressed in adipogenic cells[22]. Secondary antibodies conjugated to Alexa Fluor 647 dye (ThermoFisher Scientific) detected primary antibodies. DAPI identified nuclei. Three random 10× fields per plate were quantified in an EVOS FL Imaging System (ThermoFisher Scientific). For myogenic differentiation, a cell was considered a differentiated muscle cell if it was a multinuclear myotube or contained a nucleus that was myogenin$^+$, and myogenic cells were calculated as a percentage of total cells. For adipogenic quantification, the number of FABP4$^+$ cells per field was calculated as a percentage of total cells.

Gene Expression

Gene-expression analysis was performed as previously described[23]. RNA was isolated from cells using an miRNEasy kit (QIAGEN), reversed transcribed with iScript reagents (Bio-Rad), and amplified in a CFX96 real-time thermal cycler (Bio-Rad). Quantitative polymerase chain reaction (PCR) was performed using iTaq SYBR Green Supermix (Bio-Rad). A list of primers is shown in Appendix Table E-1. Target gene expression was normalized to the stable housekeeping gene β2-microglobulin using the $2^{-\Delta Ct}$ method.

DNA Methylation Analysis

DNA was isolated from freshly sorted tdTomato$^+$ satellite cells, and DNA methylation analysis was performed by the University of Michigan Epigenomics Core using enhanced reduced representation bisulfite sequencing (ERRBS), as previously described[24,25]. A detailed description is provided in the Appendix. Briefly, genomic DNA was digested with the methylation-insensitive restriction enzyme MspI, followed by end-repair, A-tailing, and ligation of methylated adapters. Bisulfite conversion of methylated sequences was performed prior to PCR amplification and subsequent sequencing. Gene enrichment and pathway analysis was performed with iPathwayGuide (Advaita Bioinformatics)[26]. A full list of differentially methylated regions is provided in Appendix Table E-2 and differentially methylated cytosines, in Appendix Table E-3.

Statistical Methods

Data are presented as the mean and standard deviation. Sample sizes were selected on the basis of satellite-cell myogenic differentiation rates[21]. In immunocytochemistry and gene-expression

TABLE II Top 50 Differentially Hypomethylated Regions of DNA in Satellite Cells from the Rotator Cuff Compared with the Gastrocnemius

ID	Symbol	Gene Name	Methylation Difference *(%)*	Distance *(bp)*	P Value
NR_047528	Hotair	HOX transcript antisense RNA	−65.29	5,258	0.005
NR_047528	Hotair	HOX transcript antisense RNA	−64.92	5,283	0.001
NR_047528	Hotair	HOX transcript antisense RNA	−64.29	5,308	0.001
NM_010465	Hoxc6	Homeobox C6	−61.24	12,733	0.003
NM_010465	Hoxc6	Homeobox C6	−61.14	12,808	<0.001
NR_027899	Hoxd3os1	Homeobox D3, opposite strand 1	−61.05	13,110	<0.001
NM_010465	Hoxc6	Homeobox C6	−61.03	12,833	<0.001
NM_010465	Hoxc6	Homeobox C6	−60.90	12,858	<0.001
NR_027899	Hoxd3os1	Homeobox D3, opposite strand 1	−60.74	13,135	<0.001
NM_010465	Hoxc6	Homeobox C6	−60.72	12,883	0.002
NR_027899	Hoxd3os1	Homeobox D3, opposite strand 1	−59.88	13,060	0.005
NM_010466	Hoxc8	Homeobox C8	−58.96	0	0.031
NR_027899	Hoxd3os1	Homeobox D3, opposite strand 1	−58.94	13,185	<0.001
NR_037977	Gm53	Predicted gene 53	−57.17	0	<0.001
NM_010452	Hoxa3	Homeobox A3	−56.94	0	0.015
NM_010466	Hoxc8	Homeobox C8	−56.17	0	0.005
NR_027899	Hoxd3os1	Homeobox D3, opposite strand 1	−55.79	13,235	0.002
NM_172839	Ccnj	Cyclin J	−54.26	0	0.015
NM_010451	Hoxa2	Homeobox A2	−51.90	0	0.033
NM_010466	Hoxc8	Homeobox C8	−51.73	0	0.003
NM_010451	Hoxa2	Homeobox A2	−51.06	0	0.040
NM_008274	Hoxd12	Homeobox D12	−50.78	0	0.009
NM_010465	Hoxc6	Homeobox C6	−50.04	0	0.044
NR_131758	Hoxb5os	Homeobox B5 and homeobox B6, opposite strand	−50.01	25,927	0.023
NM_010465	Hoxc6	Homeobox C6	−48.18	0	<0.001
NM_008274	Hoxd12	Homeobox D12	−47.36	0	<0.001
NM_008274	Hoxd12	Homeobox D12	−47.06	0	0.003
NM_008274	Hoxd12	Homeobox D12	−47.05	0	<0.001
NR_037977	Gm53	Predicted gene 53	−47.00	0	<0.001
NM_008274	Hoxd12	Homeobox D12	−46.63	0	0.002
NM_010465	Hoxc6	Homeobox C6	−46.52	0	0.011
NM_008274	Hoxd12	Homeobox D12	−46.48	0	0.005
NM_008274	Hoxd12	Homeobox D12	−46.38	0	<0.001
NM_008274	Hoxd12	Homeobox D12	−46.36	0	0.008
NR_037977	Gm53	Predicted gene 53	−46.34	0	<0.001
NM_008274	Hoxd12	Homeobox D12	−46.08	0	<0.001
NM_008274	Hoxd12	Homeobox D12	−46.03	0	0.012
NR_037977	Gm53	Predicted gene 53	−45.94	0	<0.001
NM_008274	Hoxd12	Homeobox D12	−45.78	0	<0.001
NR_037977	Gm53	Predicted gene 53	−45.72	0	<0.001
NR_037977	Gm53	Predicted gene 53	−45.65	0	0.001
NR_037977	Gm53	Predicted gene 53	−45.64	0	<0.001
NM_026080	Mrps24	Mitochondrial ribosomal protein S24	−45.29	11,448	0.031
NM_008274	Hoxd12	Homeobox D12	−45.27	0	0.008

continued

TABLE II (*continued*)

ID	Symbol	Gene Name	Methylation Difference *(%)*	Distance *(bp)*	P Value
NR_037977	Gm53	Predicted gene 53	−44.81	0	<0.001
NM_175730	Hoxc5	Homeobox C5	−44.42	0	0.011
NM_008274	Hoxd12	Homeobox D12	−43.48	0	0.003
NR_037977	Gm53	Predicted gene 53	−43.23	0	0.004
NM_007967	Evx2	Even-skipped homeobox 2	−43.02	15,125	0.015
NM_175730	Hoxc5	Homeobox C5	−42.62	0	0.001

experiments, differences between gastrocnemius and rotator cuff groups were assessed using a t test ($\alpha = 0.05$), with Welch correction, in Prism 7.0 (GraphPad). MethylSig R package (The Sartor Lab, University of Michigan)[27] was used for differential DNA methylation analysis using a beta-binomial approach, with p values adjusted for multiple testing using a false discovery rate (FDR) adjustment to control for type-I errors. Sites were considered differentially methylated if they had a percent change in methylation of at least 20% and an FDR-adjusted p value of <0.05.

Results

To efficiently isolate satellite cells from gastrocnemius and rotator cuff muscles, and to verify that adipogenic markers were observed in myogenic lineage cells, we used a genetic approach to label the satellite cells of $Pax7^{CreERT2}$:$R26R^{tdTomato}$ mice with tdTomato (Fig. 1-B). Across several runs, approximately 12% of cells isolated from both muscle groups were tdTomato^{+} (Fig. 1-C). We then evaluated the potential of satellite cells from the gastrocnemius and rotator cuff muscles to differentiate into myogenic and adipogenic cells ($n \geq 9$ plates analyzed per group). There was a 23% reduction in the number of differentiated rotator cuff muscle cells per field compared with gastrocnemius cells, and a 4.3-fold increase in the number of adipogenic rotator cuff cells per field (Figs. 2-A through 2-D). Next, we measured the expression of myogenesis and adipogenesis-related genes ($n \geq 6$ plates analyzed per group). While we did not see a difference between the rotator cuff and gastrocnemius groups in the early myogenic marker desmin or the muscle-fusion gene myomaker, we did see an 87% reduction in the expression of the late muscle differentiation marker MRF4 (myogenic regulatory factor 4) in rotator cuff cells (Fig. 3-A). For genes related to adipogenesis, we observed a 12-fold increase in the adipogenic transcription factor PPARγ (peroxisome proliferator-activated receptor gamma) and a 65-fold increase in FABP4 in rotator cuff cells, although no differences were observed between the rotator cuff and gastrocnemius muscle groups with respect to the adipocyte signaling molecule adiponectin or adipogenic transcription factor C/EBPα (CCAAT-enhancer-binding protein-alpha) (Fig. 3-B).

Because there was an increased capacity for adipogenic differentiation in rotator cuff cells, we sought to determine whether epigenetic differences existed between sorted gastrocnemius and rotator cuff satellite cells (Figs. 4-A and 4-B; n = 5 mice per group). We identified 180 hypomethylated regions and 175 hypermethylated regions in satellite cells from the rotator cuff compared with cells from the gastrocnemius (Fig. 4-C). The top 50 hypermethylated regions and hypomethylated regions are shown in Tables I and II. Finally, to identify biological processes and biochemical pathways that might be impacted by the difference in DNA methylation, we performed gene ontology analysis. For biological processes, the top 15 pathways identified were related to embryonic development and limb morphogenesis (Fig. 4-D). With regard to molecular function, the top pathways were related to transcription-factor activity and lipid metabolism, which is consistent with the in vitro findings related to adipogenesis.

Discussion

Satellite cells are activated after a rotator cuff tear in mice, and their biological activity is thought to play an important role in pathological changes in rotator cuff disease[28]. Meyer and colleagues found that cells from patients with partial-thickness tears had reduced proliferative capacity in vitro, but no difference in fusion, when compared with cells from untorn rotator cuff muscles and full-thickness tears[29]. In an vivo study, Lundgreen et al. reported reduced satellite cell density and fewer proliferating cells in full-thickness rotator cuff tears compared with partial tears[30]. While these studies identified differential activity of satellite cells within rotator cuff and shoulder girdle muscles in various states of injury, in the current study, we compared the activity of satellite cells from normal rotator cuff and gastrocnemius muscles, as the gastrocnemius is another commonly injured muscle that generally has better outcomes than the rotator cuff when recovering from a tendon tear[2,31,32]. We observed a reduced myogenic capacity of rotator cuff satellite cells, along with a decreased expression of the differentiated myogenic transcription factor MRF4[20]. No differences in the muscle cell-fusion gene myomaker[33] were observed, indicating a similar capacity of myogenic cells from the gastrocnemius and rotator cuff to fuse into myotubes. These results were also in agreement with a previous study of rats, which demonstrated greater fatty infiltration and reduced healing of the rotator cuff compared with the gastrocnemius[7].

There are 3 types of differentiated adipogenic cells, including white, brown, and beige adipocytes[34]. White adipose cells store fat and are the classical adipocyte cell type[35,36]. Within muscle tissue, the primary progenitor cell for white adipocytes is thought to be fibro/adipogenic progenitor (FAP) cells, which are a distinct lineage from satellite cells[35,36], although myogenic cells can also differentiate into this lineage[12,13], with debate ongoing[34]. Brown and beige adipocytes are related in function but arise from distinct populations of cells, with brown adipocytes having a myogenic origin and beige cells originating from a lineage that is likely similar to white adipocytes[34,37]. It can be difficult to morphologically discern the 3 cell types in culture; however, a common feature among all adipogenic cells is the expression of FABP4[22,38]. In our findings, all FABP4$^+$ cells were also Pax7-tdTomato$^+$, indicating that these adipocytes originated from a myogenic progenitor population. Further, we observed a 4-fold increase in adipogenic cells from rotator cuff muscles, and a 12-fold increase in the common adipogenic master regulator PPARγ, providing additional support for the finding of greater adipogenic differentiation capacity of rotator cuff satellite cells.

Numerous changes in DNA methylation were observed between rotator cuff and gastrocnemius satellite cells, and bioinformatics analysis identified several biochemical pathways involving adipogenesis and lipid metabolism that were predicted to be different between gastrocnemius and rotator cuff muscles. Many of the genes that were differentially methylated in rotator cuff samples were members of the HOX family of genes. The HOX genes encode transcription factors that were originally identified by their role in instructing the positional identity of progenitor cells along the anterior-to-posterior body axis[39]. HOX genes also play important roles in myogenesis[40], and some of the differences in HOX methylation may be related to the more proximal location of rotator cuff muscles compared with the gastrocnemius in the limb, in particular with HOX9, HOX10, HOX11, and HOX13, which display a proximal-to-distal gradient of restricted expression in the developing limb[39]. However, some of the HOX genes are also important in brown and beige adipogenesis, in particular HOXC4 and HOXC8[41]. In satellite cells from rotator cuff muscles, there were 2 hypomethylated regions for HOXC4, and 6 for HOXC8. HOXA3 has also been reported to be important in white adipogenesis[42], and 8 hypomethylated regions for HOXA3 were found in rotator cuff satellite cells. As hypomethylation of a gene is associated with an increased expression of that gene, the combined results of this study indicate that satellite cells from the rotator cuff are more likely to become adipogenic cells, and this may be explained by differential methylation of adipogenic genes.

There were several limitations to this work. Humans frequently develop more profound and severe atrophy and fat accumulation than found in mouse models of rotator cuff disease[4,43,44]. We only evaluated changes in adult male mice, which allows for examination of DNA methylation on both the X and Y chromosomes, although the observed results are likely applicable to both sexes. Differentiation experiments were performed in vitro, but it is possible that these findings do not entirely translate to the in vivo setting. We did not identify the specific type of adipocytes in our studies, but white and beige fat cells are known to be present in rotator cuff muscles[45], and there are brown fat depots located close to the rotator cuff[14,46]. We also did not evaluate changes in chromatin packaging and histone methylation, which are also epigenetic regulatory mechanisms. ERRBS analysis also focuses gene promoter regions[25], but methylation of other regions of DNA could also play important roles in regulating the activity of satellite cells. Despite these limitations, the current work provides important insight into our understanding of the cellular development of rotator cuff disease.

The rotator cuff is a clinically unique muscle group with regard to pathophysiology, surgical treatment, and rehabilitation[7,47]. In the current study, we sought to determine if satellite cells from gastrocnemius and rotator cuff muscles differ in their biological activity and epigenetic imprinting. Supporting our hypothesis, we found reduced myogenic and increased adipogenic differentiation of satellite cells from rotator cuff muscles, and differences in DNA methylation patterns that correspond to observed phenotypic differences between the 2 muscle groups, which helps to identify a cellular and genetic basis of the generally poor rates of rotator cuff muscle healing. As satellite cells are activated after injury to repair damaged muscle fibers[9], and animal models have demonstrated that the repair of chronically torn rotator cuffs causes extensive injury throughout the muscle[48], it is possible that increased differentiation of myogenic cells into the adipogenic lineage contributes to the continued accumulation of fat that is observed in many patients after rotator cuff repair[2]. Further, transplantation of satellite cells from a healthy muscle to heal diseased muscles within the same patient has shown some promise in early clinical trials[49] and has been proposed as a therapy for patients with chronic rotator cuff tears[50]. Our results provide additional support for the potential use of autologous satellite cell transplantation to improve the treatment of patients with chronic rotator cuff disease.

Appendix

eA Details of satellite cell isolation and flow cytometry, cell culture, and DNA methylation analysis and a table listing the primer sequences used for quantitative PCR; as well as tables presenting a full list of the differentially methylated regions and the differentially methylated cytosines are available with the online version of this article as a data supplement at jbjs.org (http://links.lww.com/JBJS/F35, http://links.lww.com/JBJS/F36, http://links.lww.com/JBJS/F37). ■

Note: The authors thank Claudia Lalancette, PhD, and Karthik Padmanabhan, PhD, for assistance with DNA methylation analysis, and Richard McEachin, PhD, for assistance with bioinformatics.

Manuel F. Schubert, MD, MS[1]
Andrew C. Noah, MS[1]

Asheesh Bedi, MD[1]
Jonathan P. Gumucio, PhD[1]
Christopher L. Mendias, PhD, ATC[1,2,3]

[1]Departments of Orthopaedic Surgery (M.F.S., A.C.N., A.B, J.P.G, and C.L.M.) and Molecular and Integrative Physiology (A.C.N, J.P.G., and C.L.M.), University of Michigan Medical School, Ann Arbor, Michigan

[2]Hospital for Special Surgery, New York, NY

[3]Departments of Physiology and Biophysics and Orthopaedic Surgery, Weill Cornell Medical College, New York, NY

E-mail address for C.L. Mendias: MendiasC@hss.edu

ORCID iD for M.F. Schubert: 0000-0001-9296-9801
ORCID iD for A.C. Noah: 0000-0002-2869-1005
ORCID iD for A. Bedi: 0000-0001-8926-7139
ORCID iD for J.P. Gumucio: 0000-0002-9074-3216
ORCID iD for C.L. Mendias: 0000-0002-2384-0171

References

1. Colvin AC, Egorova N, Harrison AK, Moskowitz A, Flatow EL. National trends in rotator cuff repair. J Bone Joint Surg Am. 2012 Feb 1;94(3):227-33.

2. Gladstone JN, Bishop JY, Lo IKY, Flatow EL. Fatty infiltration and atrophy of the rotator cuff do not improve after rotator cuff repair and correlate with poor functional outcome. Am J Sports Med. 2007 May;35(5):719-28. Epub 2007 Mar 2.

3. Kang JR, Gupta R. Mechanisms of fatty degeneration in massive rotator cuff tears. J Shoulder Elbow Surg. 2012 Feb;21(2):175-80.

4. Mendias CL, Roche SM, Harning JA, Davis ME, Lynch EB, Sibilsky Enselman ER, Jacobson JA, Claflin DR, Calve S, Bedi A. Reduced muscle fiber force production and disrupted myofibril architecture in patients with chronic rotator cuff tears. J Shoulder Elbow Surg. 2015 Jan;24(1):111-9. Epub 2014 Sep 3.

5. Kumar D, Karampinos DC, MacLeod TD, Lin W, Nardo L, Li X, Link TM, Majumdar S, Souza RB. Quadriceps intramuscular fat fraction rather than muscle size is associated with knee osteoarthritis. Osteoarthritis Cartilage. 2014 Feb;22(2): 226-34. Epub 2013 Dec 20.

6. Snow BJ, Wilcox JJ, Burks RT, Greis PE. Evaluation of muscle size and fatty infiltration with MRI nine to eleven years following hamstring harvest for ACL reconstruction. J Bone Joint Surg Am. 2012 Jul 18;94(14):1274-82.

7. Davies MR, Ravishankar B, Laron D, Kim HT, Liu X, Feeley BT. Rat rotator cuff muscle responds differently from hindlimb muscle to a combined tendon-nerve injury. J Orthop Res. 2015 Jul;33(7):1046-53. Epub 2015 May 13.

8. Gerber C, Schneeberger AG, Hoppeler H, Meyer DC. Correlation of atrophy and fatty infiltration on strength and integrity of rotator cuff repairs: a study in thirteen patients. J Shoulder Elbow Surg. 2007 Nov-Dec;16(6):691-6. Epub 2007 Oct 10.

9. Dueweke JJ, Awan TM, Mendias CL. Regeneration of skeletal muscle after eccentric injury. J Sport Rehabil. 2017 Apr;26(2):171-9. Epub 2016 Dec 19.

10. Hawke TJ, Garry DJ. Myogenic satellite cells: physiology to molecular biology. J Appl Physiol (1985). 2001 Aug;91(2):534-51.

11. Sincennes MC, Brun CE, Rudnicki MA. Concise review: epigenetic regulation of myogenesis in health and disease. Stem Cells Transl Med. 2016 Mar;5(3):282-90. Epub 2016 Jan 21.

12. Asakura A, Komaki M, Rudnicki M. Muscle satellite cells are multipotential stem cells that exhibit myogenic, osteogenic, and adipogenic differentiation. Differentiation. 2001 Oct;68(4-5):245-53.

13. Wada MR, Inagawa-Ogashiwa M, Shimizu S, Yasumoto S, Hashimoto N. Generation of different fates from multipotent muscle stem cells. Development. 2002 Jun;129(12):2987-95.

14. Seale P, Bjork B, Yang W, Kajimura S, Chin S, Kuang S, Scimè A, Devarakonda S, Conroe HM, Erdjument-Bromage H, Tempst P, Rudnicki MA, Beier DR, Spiegelman BM. PRDM16 controls a brown fat/skeletal muscle switch. Nature. 2008 Aug 21; 454(7207):961-7.

15. Murphy MM, Lawson JA, Mathew SJ, Hutcheson DA, Kardon G. Satellite cells, connective tissue fibroblasts and their interactions are crucial for muscle regeneration. Development. 2011 Sep;138(17):3625-37.

16. Madisen L, Zwingman TA, Sunkin SM, Oh SW, Zariwala HA, Gu H, Ng LL, Palmiter RD, Hawrylycz MJ, Jones AR, Lein ES, Zeng H. A robust and high-throughput Cre reporting and characterization system for the whole mouse brain. Nat Neurosci. 2010 Jan;13(1):133-40. Epub 2009 Dec 20.

17. Pawlikowski B, Pulliam C, Betta ND, Kardon G, Olwin BB. Pervasive satellite cell contribution to uninjured adult muscle fibers. Skelet Muscle. 2015 Dec 14;5(1):42.

18. Liu L, Cheung TH, Charville GW, Rando TA. Isolation of skeletal muscle stem cells by fluorescence-activated cell sorting. Nat Protoc. 2015 Oct;10(10):1612-24. Epub 2015 Sep 24.

19. Tseng YH, Kriauciunas KM, Kokkotou E, Kahn CR. Differential roles of insulin receptor substrates in brown adipocyte differentiation. Mol Cell Biol. 2004 Mar; 24(5):1918-29.

20. Allen RE, Temm-Grove CJ, Sheehan SM, Rice G. Skeletal muscle satellite cell cultures. Methods Cell Biol. 1997;52:155-76.

21. Mendias CL, Tatsumi R, Allen RE. Role of cyclooxygenase-1 and -2 in satellite cell proliferation, differentiation, and fusion. Muscle Nerve. 2004 Oct;30(4):497-500.

22. Shan T, Liu W, Kuang S. Fatty acid binding protein 4 expression marks a population of adipocyte progenitors in white and brown adipose tissues. FASEB J. 2013 Jan;27(1):277-87. Epub 2012 Oct 9.

23. Hudgens JL, Sugg KB, Grekin JA, Gumucio JP, Bedi A, Mendias CL. Platelet-rich plasma activates proinflammatory signaling pathways and induces oxidative stress in tendon fibroblasts. Am J Sports Med. 2016 Aug;44(8):1931-40. Epub 2016 Jul 8.

24. Akalin A, Garrett-Bakelman FE, Kormaksson M, Busuttil J, Zhang L, Khrebtukova I, Milne TA, Huang Y, Biswas D, Hess JL, Allis CD, Roeder RG, Valk PJ, Löwenberg B, Delwel R, Fernandez HF, Paietta E, Tallman MS, Schroth GP, Mason CE, Melnick A, Figueroa ME. Base-pair resolution DNA methylation sequencing reveals profoundly divergent epigenetic landscapes in acute myeloid leukemia. PLoS Genet. 2012;8(6): e1002781.

25. Garrett-Bakelman FE, Sheridan CK, Kacmarczyk TJ, Ishii J, Betel D, Alonso A, Mason CE, Figueroa ME, Melnick AM. Enhanced reduced representation bisulfite sequencing for assessment of DNA methylation at base pair resolution. J Vis Exp. 2015 Feb 24;(96):e52246.

26. Ahsan S, Drăghici S. Identifying significantly impacted pathways and putative mechanisms with iPathwayGuide. Curr Protoc Bioinformatics. 2017 Jun 27;57(1):1: 30.

27. Park Y, Figueroa ME, Rozek LS, Sartor MA. MethylSig: a whole genome DNA methylation analysis pipeline. Bioinformatics. 2014 Sep 1;30(17):2414-22. Epub 2014 May 16.

28. Davies MR, Garcia S, Tamaki S, Liu X, Lee S, Jose A, Pomerantz JH, Feeley BT. Muscle stem cell activation in a mouse model of rotator cuff injury. J Orthop Res. 2018 May;36(5):1370-6. Epub 2018 Mar 9.

29. Meyer GA, Farris AL, Sato E, Gibbons M, Lane JG, Ward SR, Engler AJ. Muscle progenitor cell regenerative capacity in the torn rotator cuff. J Orthop Res. 2015 Mar; 33(3):421-9. Epub 2015 Jan 6.

30. Lundgreen K, Lian ØB, Engebretsen L, Scott A. Lower muscle regenerative potential in full-thickness supraspinatus tears compared to partial-thickness tears. Acta Orthop. 2013 Dec;84(6):565-70. Epub 2013 Oct 31.

31. Schipper ON, Anderson RB, Cohen BE. Outcomes after primary repair of insertional ruptures of the Achilles tendon. Foot Ankle Int. 2018 Jun;39(6):664-8. Epub 2018 Feb 15.

32. Truntzer JN, Triana B, Harris AHS, Baker L, Chou L, Kamal RN. Cost-minimization analysis of the management of acute Achilles tendon rupture. J Am Acad Orthop Surg. 2017 Jun;25(6):449-57.

33. Millay DP, O'Rourke JR, Sutherland LB, Bezprozvannaya S, Shelton JM, Bassel-Duby R, Olson EN. Myomaker is a membrane activator of myoblast fusion and muscle formation. Nature. 2013 Jul 18;499(7458):301-5.

34. Schoettl T, Fischer IP, Ussar S. Heterogeneity of adipose tissue in development and metabolic function. J Exp Biol. 2018 Mar 7;221(Pt)(Suppl 1):jeb162958.

35. Joe AWB, Yi L, Natarajan A, Le Grand F, So L, Wang J, Rudnicki MA, Rossi FM. Muscle injury activates resident fibro/adipogenic progenitors that facilitate myogenesis. Nat Cell Biol. 2010 Feb;12(2):153-63. Epub 2010 Jan 17.

36. Uezumi A, Fukada S, Yamamoto N, Takeda S, Tsuchida K. Mesenchymal progenitors distinct from satellite cells contribute to ectopic fat cell formation in skeletal muscle. Nat Cell Biol. 2010 Feb;12(2):143-52. Epub 2010 Jan 17.

37. Wang W, Seale P. Control of brown and beige fat development. Nat Rev Mol Cell Biol. 2016 Nov;17(11):691-702. Epub 2016 Aug 24.

38. Carey AL, Vorlander C, Reddy-Luthmoodoo M, Natoli AK, Formosa MF, Bertovic DA, Anderson MJ, Duffy SJ, Kingwell BA. Reduced UCP-1 content in in vitro differentiated beige/brite adipocytes derived from preadipocytes of human subcutaneous white adipose tissues in obesity. PLoS One. 2014 Mar 18;9(3):e91997.

39. Pineault KM, Wellik DM. Hox genes and limb musculoskeletal development. Curr Osteoporos Rep. 2014 Dec;12(4):420-7.

40. Tsumagari K, Baribault C, Terragni J, Chandra S, Renshaw C, Sun Z, Song L, Crawford GE, Pradhan S, Lacey M, Ehrlich M. DNA methylation and differentiation: HOX genes in muscle cells. Epigenetics Chromatin. 2013 Aug 2;6(1):25.

41. Singh S, Rajput YS, Barui AK, Sharma R, Datta TK. Fat accumulation in differentiated brown adipocytes is linked with expression of Hox genes. Gene Expr Patterns. 2016 Mar;20(2):99-105. Epub 2016 Jan 26.

42. Cantile M, Procino A, D'Armiento M, Cindolo L, Cillo C. HOX gene network is involved in the transcriptional regulation of in vivo human adipogenesis. J Cell Physiol. 2003 Feb;194(2):225-36.

43. Liu X, Laron D, Natsuhara K, Manzano G, Kim HT, Feeley BT. A mouse model of massive rotator cuff tears. J Bone Joint Surg Am. 2012 Apr 4;94(7):e41.

44. Gibbons MC, Singh A, Anakwenze O, Cheng T, Pomerantz M, Schenk S, Engler AJ, Ward SR. Histological evidence of muscle degeneration in advanced human rotator cuff disease. J Bone Joint Surg Am. 2017 Feb 1;99(3):190-9.

45. Meyer GA, Gibbons MC, Sato E, Lane JG, Ward SR, Engler AJ. Epimuscular fat in the human rotator cuff is a novel beige depot. Stem Cells Transl Med. 2015 Jul;4(7):764-74. Epub 2015 May 21.

46. Jespersen NZ, Larsen TJ, Peijs L, Daugaard S, Homøe P, Loft A, de Jong J, Mathur N, Cannon B, Nedergaard J, Pedersen BK, Møller K, Scheele C. A classical brown adipose tissue mRNA signature partly overlaps with brite in the supraclavicular region of adult humans. Cell Metab. 2013 May 7;17(5):798-805.

47. Bedi A, Dines J, Warren RF, Dines DM. Massive tears of the rotator cuff. J Bone Joint Surg Am. 2010 Aug 4;92(9):1894-908.

48. Davis ME, Stafford PL, Jergenson MJ, Bedi A, Mendias CL. Muscle fibers are injured at the time of acute and chronic rotator cuff repair. Clin Orthop Relat Res. 2015 Jan;473(1):226-32. Epub 2014 Aug 12.

49. Yiou R, Hogrel JY, Loche CM, Authier FJ, Lecorvoisier P, Jouany P, Roudot-Thoraval F, Lefaucheur JP. Periurethral skeletal myofibre implantation in patients with urinary incontinence and intrinsic sphincter deficiency: a phase I clinical trial. BJU Int. 2013 Jun;111(7):1105-16. Epub 2013 Mar 7.

50. Patel S, Gualtieri AP, Lu HH, Levine WN. Advances in biologic augmentation for rotator cuff repair. Ann N Y Acad Sci. 2016 Nov;1383(1):97-114. Epub 2016 Oct 17.

51. Krueger F, Andrews SR. Bismark: a flexible aligner and methylation caller for Bisulfite-Seq applications. Bioinformatics. 2011 Jun 1;27(11):1571-2. Epub 2011 Apr 14.

52. Langmead B, Salzberg SL. Fast gapped-read alignment with Bowtie 2. Nat Methods. 2012 Mar 4;9(4):357-9.

53. Rosenbloom KR, Armstrong J, Barber GP, Casper J, Clawson H, Diekhans M, Dreszer TR, Fujita PA, Guruvadoo L, Haeussler M, Harte RA, Heitner S, Hickey G, Hinrichs AS, Hubley R, Karolchik D, Learned K, Lee BT, Li CH, Miga KH, Nguyen N, Paten B, Raney BJ, Smit AF, Speir ML, Zweig AS, Haussler D, Kuhn RM, Kent WJ. The UCSC Genome Browser database: 2015 update. Nucleic Acids Res. 2015 Jan;43(Database issue):D670-81. Epub 2014 Nov 26.